

Phase separation of binary mixtures induced by soft centrifugal fields†

Thomas Zemb,^a Rose Rosenberg,^b Stjepan Marčelja,^c Dirk Haffke,^b Jean-François Dufrêche,^a Werner Kunz,^d Dominik Horinek^{*d} and Helmut Cölfen^b

We use the model system ethanol–dodecane to demonstrate that giant critical fluctuations induced by easily accessible weak centrifugal fields as low as 2000g can be observed above the miscibility gap of a binary liquid mixture. Moreover, several degrees above the phase transition, *i.e.* in the one-phase region, strong gradients of ethanol concentration occur upon centrifugation. In this case, the standard interpretation of sedimentation equilibrium in the analytical ultracentrifuge (AUC) yields an apparent molar mass of ethanol three orders of magnitude higher than the real value. Notably, these composition gradients have no influence on the distribution gradient of solutes such as dyes like Nile red. The thick opaque interphase formed upon centrifugation does not appear as the commonly observed sharp meniscus, but as a turbidity zone, similar to critical opalescence. This layer is a few millimeters thick and separates two fluids with low compositional gradients. All these effects can be qualitatively understood and explained using the Flory–Huggins solution model coupled to classical density functional theory (DFT). In this domain hetero-phase fluctuations can be triggered by gravity even far from the critical point. Taking into account Jean Perrin’s approach to external fields in colloids, a self-consistent definition of the Flory effective volume and an explicit calculation of the total free energy per unit volume is possible.

Introduction

Jean Perrin measured the Avogadro number by analysing concentration gradients in the supernatant “atmosphere” of colloids above a close-packed colloidal crystal. In his Nobel prize winning work, the “atoms” used were monodisperse solidified gum emulsion droplets of colloidal size in “atmospheric” equilibrium under gravity.¹ Since then, several works have used osmotic pressure in a dispersion of colloids in order to measure colloidal forces. Measured osmotic pressures in colloidal dispersions differ markedly from what would be expected from the standard DLVO paradigm combining electrostatics and dispersion forces. Therefore, colloidal interactions such as hydration as well as depletion forces need to be taken into account in order to obtain coherent descriptions of the equation of state of colloids.^{2,3} The

additivity of weak long-range interactions in soft matter was always assumed and not contradicted by experimental results. Following systems were studied:

- electrostatics of colloidal crystals based on latex in equilibrium with nanomoles of ribonucleic pentavalent salt as co-ions⁴
- microemulsions with a g-dependent miscibility gap⁵
- lamellar liquid crystals as a situation allowing access to undulation forces⁶
- extremely dilute microemulsions in Earth’s gravity field.⁷
- direct and safe establishment of the equation of state of synthetic clays, difficult to obtain *via* classical methods based on dialysis instead of AUC.⁸ Strange and yet unexplained behaviour in AUC has been discovered by Barden and co-workers in the seventies,⁹ which was qualitatively attributed to “surfactant-free microemulsions” alias “ultraflexible microemulsions (UFME)”.

Before trying to understand the behaviour of UFME under centrifugal fields, a preliminary question occurs: What is the behaviour of a binary mixture “near” and “far” from its critical composition in a sedimentation field? In a binary mixture, no interfacial film can be formed by a third surface-active component.

Gravity is known to play a crucial role near the critical point of liquid mixtures.^{10,11} Hildebrand and co-workers described in

^a *Institute for Separation Chemistry ICSM U Montpellier/CEA/CNRS/ENSCM, Marcoule, France*

^b *Physical Chemistry, Department of Chemistry, University of Konstanz, Universitätsstr. 10, D-78457 Konstanz, Germany*

^c *Applied Maths, RSPHys, ANU, ACT 2601, Canberra, Australia*

^d *Institute of Physical and Theoretical Chemistry, University of Regensburg, D-93040 Regensburg, Germany. E-mail: dominik.horinek@ur.de*

1954, a slight difference of the order of 0.2 °C in the critical temperature in the vicinity of the critical composition upon application of a centrifugal field. Several papers discussed this problem and the possible underlying mechanism. In 1985, Rossen, Davies, and Scriven, concluded that this temperature effect was an artefact and that instability could be mixed up with fluctuations near a critical point in a binary mixture.¹² Finally, Winnik, Knobler and Scott concluded in 1989¹³ that “Both the density inversion and the stretching of the correlation length may occur, but, since both models have proportionality constants of uncertain magnitude, they may be of less importance than their proponents originally believed.”: the scientific question is still open, thirty years after this paper. To the best of our knowledge, no description and quantitative rationalization of the behaviour of a hydrotrope-alkane mixture under centrifugation has been published since then.

This motivated our interest in revisiting the behavior of a binary solution in the presence of a centrifugal field, both “far” and “close” to the critical point, systematically comparing the effect of temperature variation and centrifugal field on all samples. We chose ethanol (EtOH) as the most common hydrotrope and *n*-dodecane (*n*C12) as the solvent, because it is well documented and of practical importance. Moreover, the critical temperature is easily accessible. Moreover, we added a dye as solute and measured its partition coefficient after phase transition. In the monophasic region close to the phase transition temperature (T_s), we measured the distribution of the dye in the AUC measurement cell.

Experimental methods and techniques

Chemicals

H-ethanol (EtOH, purity $\geq 99.9\%$) was purchased from Merck KGaA (Darmstadt, Germany) and *n*-dodecane (*n*C12, purity $\geq 90.0\%$) was purchased from Fluka Chemie GmbH (Buchs, Switzerland). D-ethanol (EtOD, 99.0 atom %D) and Nile red (NR, technical grade) were purchased from Sigma-Aldrich Chemie GmbH (Steinheim, Germany). All chemicals were used without further purification.

Establishment of the binary phase diagram

For the determination of the binary phase diagram (BPD), the binary mixtures were prepared by weighing masses of about 1 g to ± 0.1 mg on an analytical balance. The samples were prepared in crimp neck vials N11 (\varnothing 11 mm, 1.5 ml, clear glass) with crimp caps aluminium. Ethanol was added dropwise with a micropipette to the dodecane from 85/15 to 40/60 dodecane/ethanol ratios by weight. For the samples with Nile red, a 0.0261 mM ethanol-dye stock solution was prepared. The method of determination of Nile red concentration is available in the ESI.†

A four crimp neck vials with the samples were placed in a water/ethylene glycol bath at 295.15 K and tempered for two hours before the cooling process was started. To determine the solution temperature of the samples, a precision Pt100 temperature sensor of the Refrigerated Circulator F26 (JULABO GmbH, Germany) was placed close to the vials in the centre. After starting

the cooling process with the Refrigerated Circulator, the temperature of the water/ethylene glycol bath was read out with a LabVIEW program (LabVIEW 2018, 32 bit from National Instruments) developed by one of us (D. Haffke). As soon as the solution temperature was changed by 0.1 °C, an image was taken with a Canon EOS 6D camera using LabVIEW programmed control. From these images, the demixing temperature of the liquid-liquid separation was taken for each solution and represented in Fig. 2 as “BPD UniKon” points of ethanol/dodecane mixtures and as “BPD UniKon + NR” points of EtOH + Nile red/*n*C12 mixtures. The complete equipment setup and the video links of the transition temperature are available in the ESI.†

Analytical ultracentrifugation

For the measurements, the dodecane/ethanol mixtures with 80/20 and 60/40 wt% ratios were selected from the binary phase diagram. The samples were prepared in the same way as for the binary phase diagram.

The measurements were performed on a modified Optima XL 80k (Beckman Coulter, Palo Alto, CA, United States) using an UV/Vis multiwavelength (MWL) detector¹⁴ and an advanced Rayleigh interference optics developed by Nanolytics.¹⁵ The general setup of the MWL technique is described ref. 16 and 17. A 12 mm double sector titanium centrepiece was used as a measurement cell with 360 μ l of *n*C12 as reference solution and 355 μ l of mixed binary solution in the sample sector. The temperature variation experiments between 22 °C and 11 °C were performed at 5000 rpm. The speed variation experiments were performed at 19 °C temperature with speeds between 2000 and 40 000 rpm, which have no measurable effect on the temperature of the sample.

The raw data were presented using OriginLab 2019¹⁸ and a self-written LabVIEW¹⁹ program.

The experimentally obtained interference fringe pattern is the result of a Fourier transform analysis.²⁰ The vertical shift of the interference fringes is counted in numbers $J(r)$ of fringes and is defined by Mächtle and Börger²¹

$$J(r) = \frac{\Delta n(r) \times a}{\lambda} \quad (1)$$

where a is the thickness of the centerpiece (1.2 cm), λ is the wavelength of the laser light (675 nm), and $\Delta n(r)$ is the refractive index difference given as:

$$\Delta n(r) = n_{\text{solution}}(r) - n_{\text{solvent}}(r) \quad (2)$$

From eqn (4), the refractive index profile $n(r)$ at each radius position r can be calculated:

$$\Delta n(r) = \frac{J(r) \times \lambda}{a} = 5.625 \times 10^{-5} \times J(r) \quad (3)$$

However, if a meniscus or turbid zone occurs in the interference pattern as shown in Fig. 12, the phase information gets lost in the Fourier transformed data at this position. This results in the loss of the correct fringe shift information and this data is not useable anymore for the calculation of the refractive index or concentration profile of the respective sample. Such turbid zones occur in several of our experiments and we refer to their occurrence in

the respective figure/discussion. In such cases, the experimental profiles as presented appear rather flat, but this does not imply a nearly constant actual volume fraction profile. On the contrary, a jump in composition can be hidden in such a profile.

For a binary system, a conventional volume mixing rule can be applied:²²

$$n_{\text{solution}} = \varphi_1 n_1 + \varphi_2 n_2 \quad (4)$$

where n is the refractive index of solution, 1 for the solvent fraction of the solution, and 2 for the solute (EtOH), and φ is the volume fraction of the respective components. With $\varphi_1 = 1 - \varphi_2$ follows:

$$n_{\text{solution}} = (1 - \varphi_2)n_1 + \varphi_2 n_2 = \varphi_2(n_2 - n_1) + n_1$$

$$\varphi_2 = \frac{n_{\text{solution}} - n_1}{n_2 - n_1} \text{ or } \varphi_{\text{solute}} = \frac{n_{\text{solution}} - n_{\text{solvent}}}{n_{\text{solute}} - n_{\text{solvent}}} \quad (5)$$

The combination of (2) and (5) leads to the following expression, and the small volume fraction difference of ethanol can be directly calculated from the experimentally obtained interference data:

$$\Delta\varphi(r)_{\text{solute}} = \frac{\Delta n(r)}{n_{\text{solute}} - n_{\text{solvent}}} \quad (6)$$

In order to obtain the volume fraction profile $\varphi(r)$, the position r of the initial concentration of the mixture $\varphi_{\text{solute}}^0$ must be known. This point can be found by searching the r position for which the integrals of $\varphi(r)_{\text{solute}}$ for smaller and larger r are equal (see Fig. 1 for an illustration).

From eqn (6), the volume fraction profile $\varphi(r)$ of the solute at each radius position can be calculated:

$$\varphi(r)_{\text{solute}} = \Delta\varphi(r)_{\text{solute}} + \varphi_{\text{solute}}^0 \quad (7)$$

where the superscript 0 defines the volume fraction of the components prior to mixing, $\varphi_i^0 = V_i^0 / \sum V_i^0$.

The fundamental equation to determine an apparent weight-average molar mass at a radial distance $M_{w,\text{app}}(r)$ at sedimentation equilibrium in a centrifugal field is given by

$$M_{w,\text{app}}(r) = \frac{1}{k} \cdot \frac{d(\ln c(r))}{d(r^2)} = \frac{1}{k} \cdot \frac{(dc/dr)}{2c(r)\Delta r} \quad (8)$$

where $k = (1 - \bar{v}_2 \rho_1) \omega^2 / 2RT$, \bar{v}_2 is the partial specific volume of the solute, ρ_1 is a solvent density, ω is the angular velocity, R is the gas constant, T the thermodynamic temperature, c is the concentration, and r is the radial distance from the center of rotation.

The concentration profile $c(r)$ can conveniently be replaced by $\varphi(r)$, which is known from eqn (7) so that the equation for the determination of the molar mass from the radial concentration profile $\varphi(r)$ reads:

$$M_{w,\text{app}}(r) = \frac{1}{k} \cdot \frac{d(\ln \varphi(r))}{d(r^2)} \quad (9)$$

Flory–Huggins modeling of a binary fluid in a gravitational field

The phase changes of binary fluids exhibit the same universal behaviour as other first-order phase transitions where two variables control the state of the system. For example, in liquid–vapour phase transition the pressure and temperature are most often

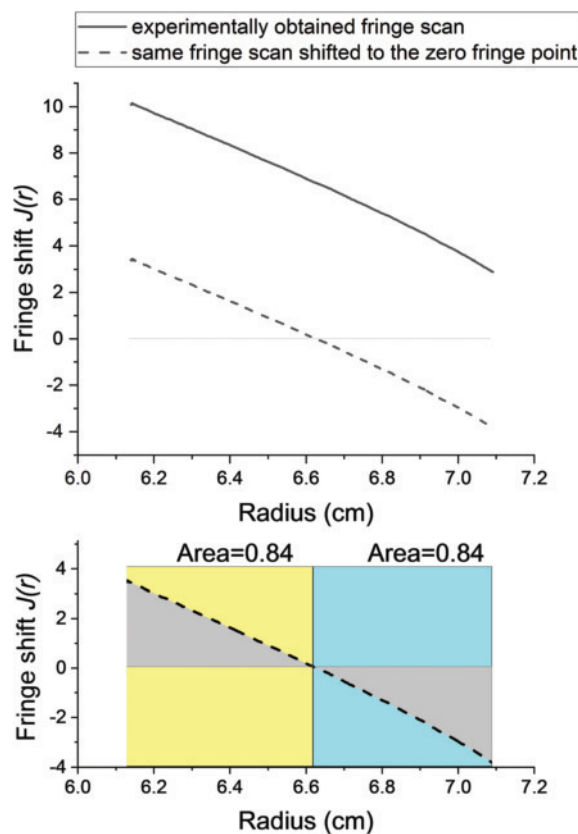


Fig. 1 Illustration of the relation between fringe scan results and system compositions. Top: Demonstration of an experimentally obtained fringe scan (solid line) and the same scan shifted to the zero fringe point ($J = 0$, $c = 0$) (dashed line). Bottom: Demonstration that the two resulting grey areas in the yellow and blue region are equal.

chosen as the controlling variables. In the case of binary fluids, the controlling variables are temperature and composition. Increasing temperatures lead to a phase transition from a binary fluid to a single phase. If volume fractions are at the critical value, a critical point is reached where properties of the two phases are no longer distinguishable. Near this point the system density or composition exhibit strong fluctuations observed as a critical opalescence.

Under the influence of a strong gravitational force in a centrifuge, a binary fluid develops density gradients. It should be expected that in order to minimise the free energy the phase behaviour in the sample will change, favouring full or partial phase separation. Modelling of ultracentrifugation requires two theoretical ingredients. First, the free energy of the mixture has to be determined in order to describe the (equilibrium) thermodynamical properties of the solution. Ethanol/dodecane mixtures are not ideal and excess terms are expected. In order to quantify these phenomena we used the Flory–Huggins (FH) model of binary fluids.²³ This model was chosen because it produces qualitatively correct results despite its simplicity. It should be noted that the universality, which is known to be valid across many physically different systems applies to the phase transitions under centrifugation, and therefore our results do not depend on the model or on the particular kind of the first-order phase transition selected.

The second ingredient is required to couple the effect of the centrifugation field to the solution. This can be done with the use of the classical Density Functional Theory (DFT)^{24,25} (see the ESI† for a derivation). Several functionals can be used to describe inhomogeneous systems. For the sake of simplicity, we considered the Local Density Approximation (LDA) functional. The latter is valid if the scale of density variations is much larger than the size of the molecules.

The symmetric FH model was used earlier to describe the centrifugation of symmetric polymer mixtures below the critical point but above the binodal.²⁶ Here, we needed to model the

ethanol-dodecane binary fluid and hence used the full FH Gibbs energy

$$G_{\text{FH}} = k_{\text{B}}T(N_1 \ln \varphi_1 + N_2 \ln \varphi_2 + N_1\varphi_2\chi),$$

with the number of molecules N_i and the volume fractions $\varphi_1 = N_1/N$ and $\varphi_2 = r^{\text{FH}}N_2/N$. The interaction parameter χ and the ‘number of monomers’ r^{FH} are fixed to reproduce the ethanol/dodecane experimental phase diagram²³ (see Fig. 2 for details). Within the LDA, in the gravitational field of the centrifuge rotating at an angular velocity ω , the free energy functional is written as the integral of the free energy density $f(r)$ over the radial coordinate r (radius). The numbers of molecules N_i are integrals over the number densities $N_i(r)$, and $\varphi_i(r)$ are local volume fractions. The effect of the sedimentation field can be expressed by a similar integral that depends on the centrifugation energy potential $m_i\psi_G = -\frac{m_i\omega^2 r^2}{2}$ with the angular velocity ω and the molecular masses m_i . The number density profiles follow from a variational minimization of the free energy functional.⁶

The detailed calculations are given in the appendix. The final equation for the ethanol volume fraction $\varphi_1(r) = \varphi$ is

$$k_{\text{B}}T \left[\ln \varphi - \frac{1}{r^{\text{FH}}} \ln(1 - \varphi) + 1 - \frac{1}{r^{\text{FH}}} + \chi - 2\varphi\chi \right] - \frac{1}{2}\Delta v_0\omega^2 r^2 + \mu = 0 \quad (10)$$

where $\Delta\rho$ is the difference in mass density of the two components and v_0 the solvent volume. The Lagrange multiplier μ corresponds to the chemical potential. Eqn (10) can be solved numerically for $\varphi(r)$ where μ is obtained by the condition that the integral over $\varphi(r)$ gives the correct total volume fraction.

Composition fluctuations are in general related to changes in chemical potential according to²⁷

$$\langle \Delta N^2 \rangle \sim \left(\frac{\partial \mu}{\partial \varphi} \right)^{-1}. \quad (11)$$

The derivative in eqn (11) giving the dependence of the chemical potential μ on the r -dependent composition φ in the centrifuge is evaluated from the FH expression for the chemical potential (see Flory’s book, ref. 23, eqn (XII.26) or (XIII.3)).

$$\frac{\partial \mu}{k_{\text{B}}T\partial \varphi} = \frac{1}{1 - \varphi} - \left(1 - \frac{1}{r^{\text{FH}}} \right) - 2\varphi\chi. \quad (12)$$

Experimental results

In this study we chose two compositions (60/40 ‘close’ to the critical point and 80/20 far from the critical point dodecane/ethanol ratios by weight). Determined by weak centrifugation, the 60/40 ratio of nC12/EtOH is close to the critical point that occurs at 13 °C without Nile red as dye and 15 °C with the presence of solute. To enhance buoyancy monodeuterated (D) ethanol was used in some cases.

Fig. 2 shows the two compositions investigated *versus* the single-phase to two-phase transition temperature. The phase

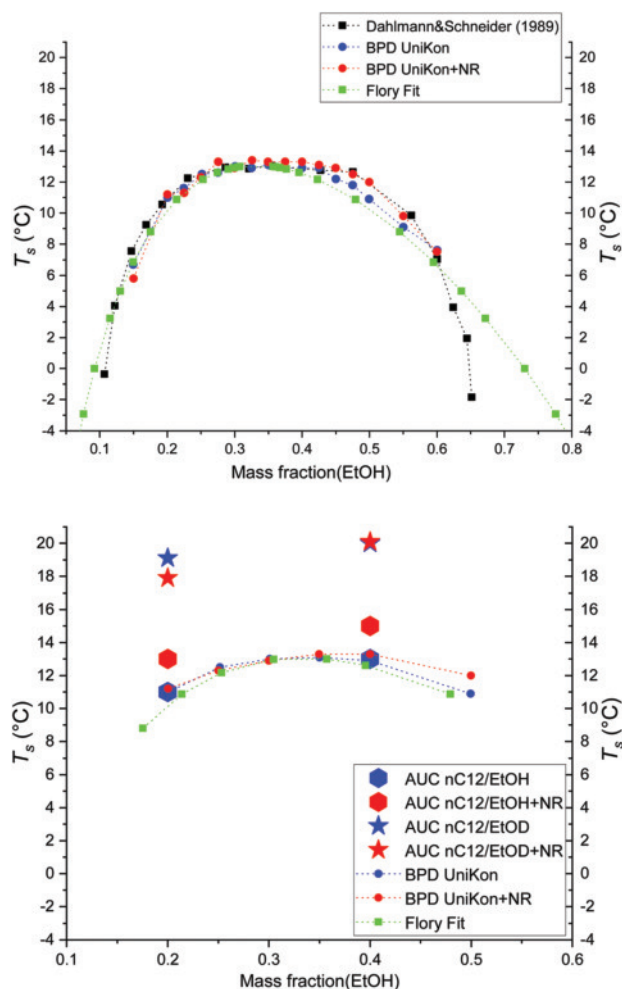


Fig. 2 Single phase to two phases transition temperature (T_s) of EtOH/ n C12 mixtures. Top: The phase diagram reconstructed from ref. 34 is shown with black cubes. The phase separation of exactly the same mixing ratios without (blue spheres) and with the addition of Nile red dye (red spheres) was experimentally reproduced at the University of Konstanz (BPD UniKon). Also shown is the fit of the Flory model with green cubes (The fit parameters are dodecanol/ethanol molecular volume ratio $x = 1.5$ and the Flory interaction parameter ($\chi = b/T - a$, with $a = 211.5$ and $b = 123.2$)). Bottom: To the T_s established in this study from BPD experiment and the Flory model fit, the T_s are represented from experimental results determined by analytical ultracentrifugation (AUC) in this study (unconnected stars and hexagons). Composition and deuteration of samples are indicated.

diagram reported in literature, shown in Fig. 2 (top) as black cubes connected with a dotted line, was taken from ref. 34. The critical point occurring at 15 °C for H-ethanol and for D-ethanol at 20.1 °C in the presence of dye is also indicated in the figure. All experimental data taken at the University of Konstanz determined by binary phase diagram experiments (BPD UniKon points) and by analytical ultracentrifugation experiments (AUC points), are also shown in Fig. 2.

The single-phase to two-phase transition temperature with and without solute is also indicated. In the following, data are always considered in temperature difference with the phase boundary for the given deuteration level of ethanol. Fig. 3 shows the effect of temperature on the sedimentation equilibrium at constant speed. Temperature is decreased by small 1 °C steps and a delay of typically 24 h is imposed until the sedimentation equilibrium is reached while the actual temperature is recorded in 0.1 °C steps. At an initial temperature a few degrees Celsius above the demixing temperature, strong gradients are seen in the single-phase domain. This well-known phenomenon²⁸ is intense close to the critical composition and temperature of phase separation, but surprisingly still noticeable far in composition from the critical point as shown on the left side of Fig. 3. Significant effects even far from critical points are expected and well described when one of the

components is an aqueous salt solution made from two ions of any size and a non-miscible solvent,²⁹ but the result obtained “far” from the critical composition *i.e.* as much as 40 wt% of ethanol away from the critical point is surprising. Analysis of the ethanol equilibrium concentration gradients by routine expressions used in AUC would lead to inconsistent results that will be discussed later.

Moreover, in binary systems, it is not possible to observe a hetero-phase critical fluctuation³⁰ that could be triggered by giant fluctuations due to organisation of a third surface-active component even far from critical composition. Therefore, our initial driving question becomes now: What is the mechanism of the molecular force equilibrium at the origin of the gradients observed as much as 2 °C above the phase separation? This composition gradient disappears within each of the two phases when the phase separation occurs. Presence of a well-defined meniscus is seen as some irregularity near the meniscus that separates the two phases.

The gradient disappears below the upper critical solution temperature (UCST). The phenomenon is independent of the presence of a dye of moderate buoyancy, as can be seen by comparing the top and bottom of Fig. 3.

Turning now to Fig. 4 on the right column, we can compare the effect obtained by decreasing temperature with the effect

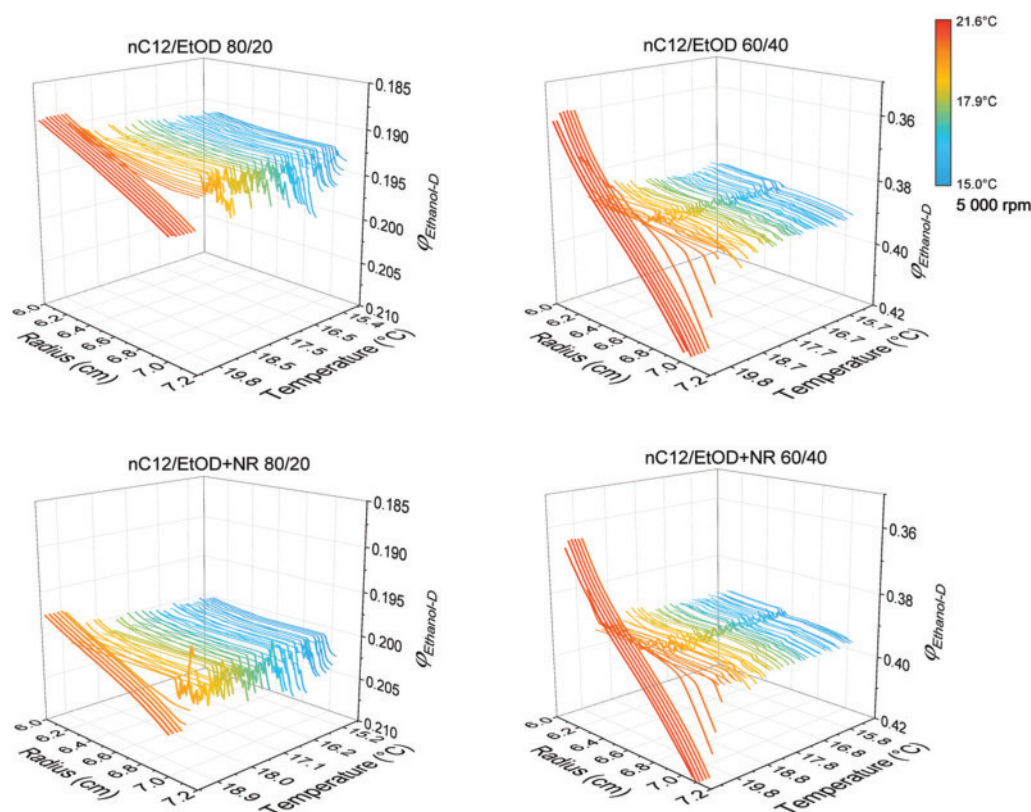


Fig. 3 AUC experimental results: Ethanol volume fraction versus radius and temperature as indicated far from the critical point (left) and close to the critical point (right) without Nile red dye (top) and with the presence of tracer amount of Nile red (bottom). The strong composition gradients formed above the phase separation temperature disappear below the UCST. The fluctuation instability corresponding to the centrifuge-induced criticality is easily seen present as a wide band present two degrees Celsius above phase separation. The speed is constant (5000 rpm). When this zone appears, the real volume fraction profile within the turbid zone cannot be detected.

obtained increasing the external centrifugal field. The speed is progressively increased. This corresponds to an increased centrifugal field at the bottom of the analytical cell from 320g at 2000 rpm to 127 500g at 40 000 rpm. The behavior under increasing centrifugal field observed is qualitatively similar to that observed for temperature variation, but differs in appearance since the centrifugal field, unlike temperature, is not constant along the AUC cell. At low speeds, no gradients are seen.

For a composition close to the critical point, strong gradients emerge in the single phase. With a further increase in speed, instead of the thin meniscus observed in the temperature variation experiment, one observes a wide (few mm) region of turbid zone. This turbid zone can be understood as a type of critical opalescence induced by the external field. To our knowledge, the existence of this turbid zone in ternary systems was reported for the first time by Barden and coworkers, but without any possible explanation of this spontaneous emulsification phenomenon. This turbid zone remains present even at the highest sedimentation speed that can be reached, *i.e.* up to a gravity of 2 90 000g. Fig. S1–S3 in the ESI† demonstrate the minor effect of the presence of the Nile red dye on the ethanol concentration profiles.

Performing now the same experiment, gradual speed increase with delay to allow equilibrium, at the composition

far from the critical point ($nC12/EtOH$ 80/20), we see in Fig. 4 (left column) the same increase of the gradient obtained by decreasing temperature in the single-phase domain. A comparison of gradients close and far from the critical composition is shown in Fig. S4 in the ESI.† But this time, the phase separation occurs first at the bottom of the tube where the centrifugal field is the strongest. And again, the broad turbid zone shown by the arrow “replaces” the meniscus between the two fluids in coexistence. The presence of Nile red shifts the USCT upwards but does not change the overall behaviour noticeably: The top and bottom experimental results obtained in the absence or in the presence of a dye as model solute are similar. This illustrates that the free energy of the binary solution is not changed by the small amount of model solute present. In principle, the gradient of the dye, as a solute in a mixture, should modify the interaction between solute molecules (ethanol in our case) if detectable by more refined experiments. The effect of preferential solvation as introduced by Ben Naim³¹ could be accessed by introduction of a “non-trivial term” into the equation of state as proposed by Hansen and co-workers for the case of colloids in polymer solutions.³²

Fig. 5 shows the optical density (OD, we use the term “optical density” for absorbance) observed when a minute amount of Nile red dye is added for a composition near the critical point (see experimental methods part). The rotation

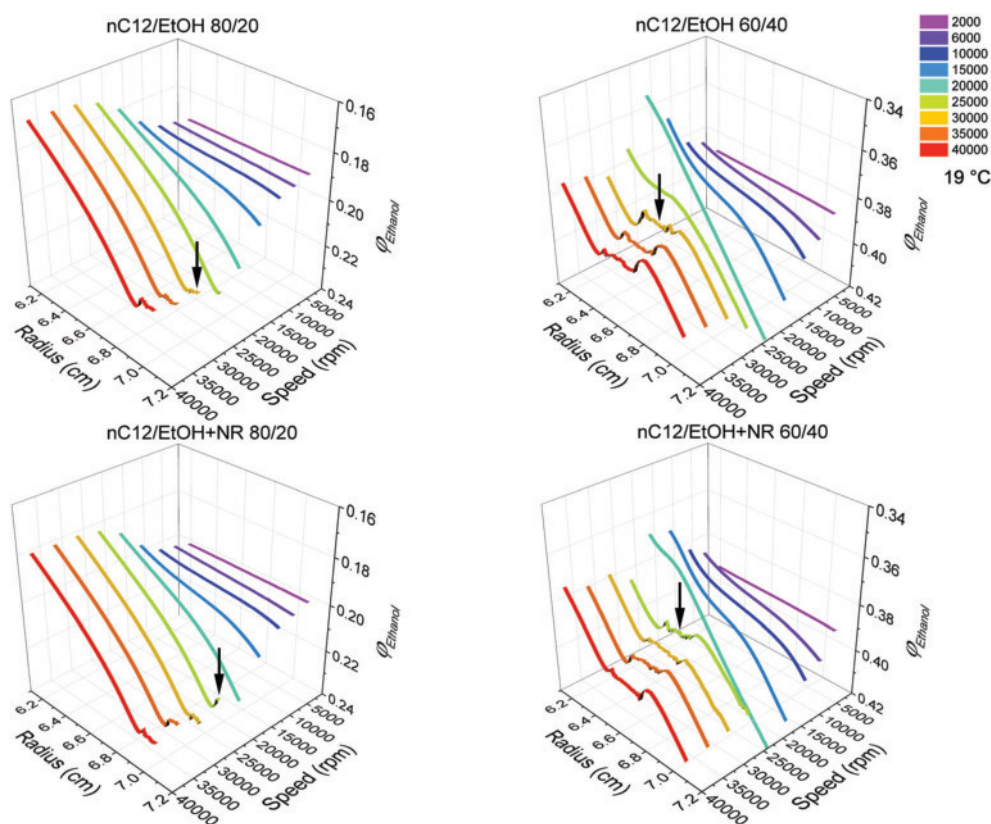


Fig. 4 Same experiment as shown in Fig. 3, but this time the speed is varied. The gravity field is increased in steps, waiting between steps until sedimentation equilibrium is reached. The diffuse band corresponding to centrifuge induced criticality is observed above 20 000 rpm. For details on the calculation of ϵ and c for Nile red see the ESI.† The temperature is 19 °C. The broad turbid zones observed are marked with a black arrow. When this zone appears, the real volume fraction profile within the turbid zone cannot be detected.

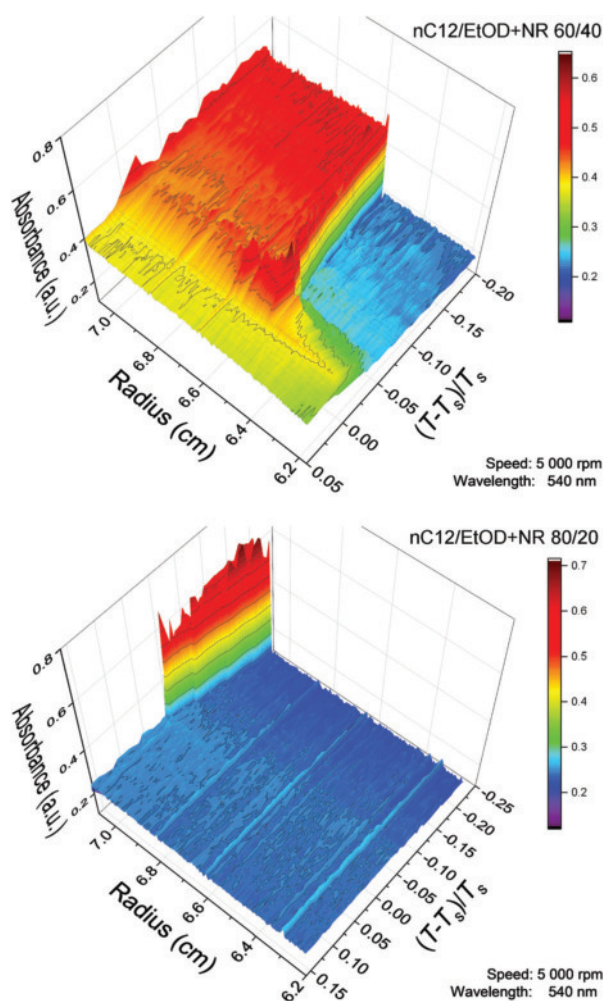


Fig. 5 Concentration gradient of the dissolved dye for different reduced temperatures, $(T - T_s)/T_s$ at a speed of 5000 rpm, near the critical composition (top) and far from it (bottom). Below the phase transition temperature T_s , the partition coefficient of the dye between the ethanol-rich and the dodecane-rich phase can be directly taken from the OD values of the two phases.

speed of the sample is also 5000 rpm and the OD was taken at the isosbestic wavelength, when the absorption coefficient does not depend on the polarity of the solvent (540 nm). The data is shown in reduced temperature, $(T - T_s)/T_s$. In the two-phase regime there is no gradient in dye. More than two degrees above the phase separation temperature there is also no gradient. Less than two degrees above phase separation temperature there is a region with high optical density which is not linked to the concentration of the dye, but to the opalescence inherent to the centrifuge-induced criticality (see Fig. S5 in the ESI†).

This coexistence of concentration gradients with fluctuation of concentration that diverge near the critical point was predicted theoretically near to the critical point of a binary solution.¹² To the best of our knowledge, no experimental report on real solution far from the critical point of any binary solution has been reported yet. Moreover this centrifuge-induced criticality is also visible far from the critical point. This occurs above the phase transition temperature and is not expected for a small

molecule (molar mass = 318 g mol⁻¹) in a single-phase binary solution unless there are organized microstructures in the system. Examples for such microstructures are ethanol/alkane mixtures.³³ The noisy data visible in Fig. 3–5 is a consequence of the interference occurring in the opalescent region located above the meniscus separating the two demixed phases.

When the phase separation is achieved, there is a sharp step in OD, while there is no gradient in each of the phases (see Fig. S6 in the ESI†). The ratio of OD allows access to the difference in free energy of solvation of the dye between the ethanol-rich and the dodecane-rich phase. The OD ratio (decimal logarithm) is of the order of 0.62. So the chemical potential difference in the mole fraction scale is $1.5 k_B T$ or 3 kJ mol⁻¹.³⁴ Fig. 6 shows the AUC experimental results obtained *via* the temperature scans. The Y-axis is translated into volume fraction of ethanol *via* integration of the fringes (see Experimental description).

A few degrees above the phase separation temperature, strong gradients with a concentration range spanning even above 5% of ethanol are obtained. This effect is not linked to any temperature gradient, which can be seen by comparing the top and bottom part of the figure. Fig. 6 compares the ethanol concentration profiles close the critical point and far from the critical point. The three main features are qualitatively the same:

- A steeper concentration profile established in single phase regions above T_s , which is referred as concentration gradient.
- A turbid zone is sometimes detected close to the region where a meniscus finally appears.
- There is no detectable gradient in concentration within each of the two phases once the two phases have separated in ethanol-rich and dodecane-rich phases.

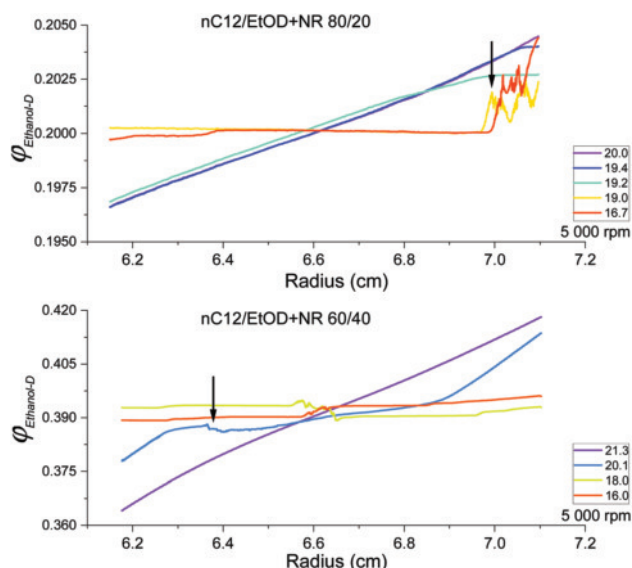


Fig. 6 Comparison of the ethanol volume fraction profiles obtained far from the critical point, with a volume fraction of 20% of ethanol (top) and close to the critical point *i.e.* a composition of approximately 40% volume fraction of ethanol (bottom). The temperatures in °C for each sample are indicated. As soon as phase separation occurs, a turbid zone can be detected, which transforms into a meniscus between the two separated phases. In this case, the real volume fraction profile within the turbid zone cannot be detected.

However, the magnitudes of gradients observed are typically a factor of five stronger close to the critical point. All effects are measured only less than 2 °C above the T_s .

Fig. 7 compares the results of the speed increase to the step cooling experiment, translating raw data shown also in into volume fraction of ethanol (as in the Fig. 6). A significant variation of typically to 3% over the length of the AUC cell is obtained at moderate speed (5000 rpm).

This would be the order of magnitude for a medium molar mass polymer. The effect is increasing until 20 000 rpm. Above this speed and at 19 °C, a turbid zone suddenly appears near the middle of the tube, while the gradients observed above and below stay the same as they were.

This large turbid zone that is not observed without centrifugal field is located between 6.3 and 6.6 cm radius. The optical appearance of this effect triggered by the centrifugal field is reminiscent of critical opalescence. This effect is NOT observed *via* a temperature scan at low speed, because there is no centrifuge-induced criticality at 5000 rpm. When the centrifuge speed is insufficient for inducing centrifuge induced criticality, the effect of temperature variation is qualitatively the same as that of speed variation, as shown in Fig. 7. This equivalence is a general route to quantitatively measure nonidealities by variations of known external fields. This applies generally to binary molecular solutions as a simple method developed originally for the study of interacting micron-sized emulsion droplets.³⁵

Discussion using Flory–Huggins theory

First, we discuss the experimental results in the framework of the FH theory. The determination of the FH interaction

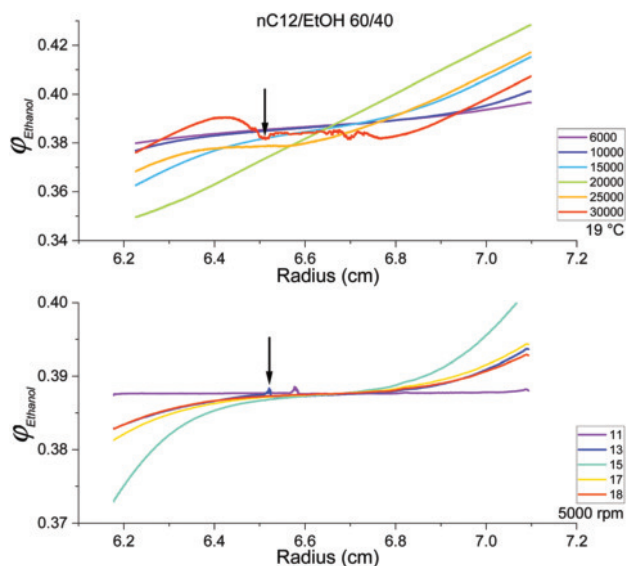


Fig. 7 The speed variation experiment (top) compared to the temperature variation experiment (bottom) for the sample close to the critical point. Speeds and temperatures in °C are indicated in the figure. As soon as phase separation occurs, a turbid zone can be detected, which transforms into a meniscus between the two separated phases. In this case, the real volume fraction profile within the turbid zone cannot be detected.

parameter from experimental data is shown in Fig. 2. Fig. 8 shows expected profiles of the ethanol volume fraction along the radial axis in the centrifuge for different experimental

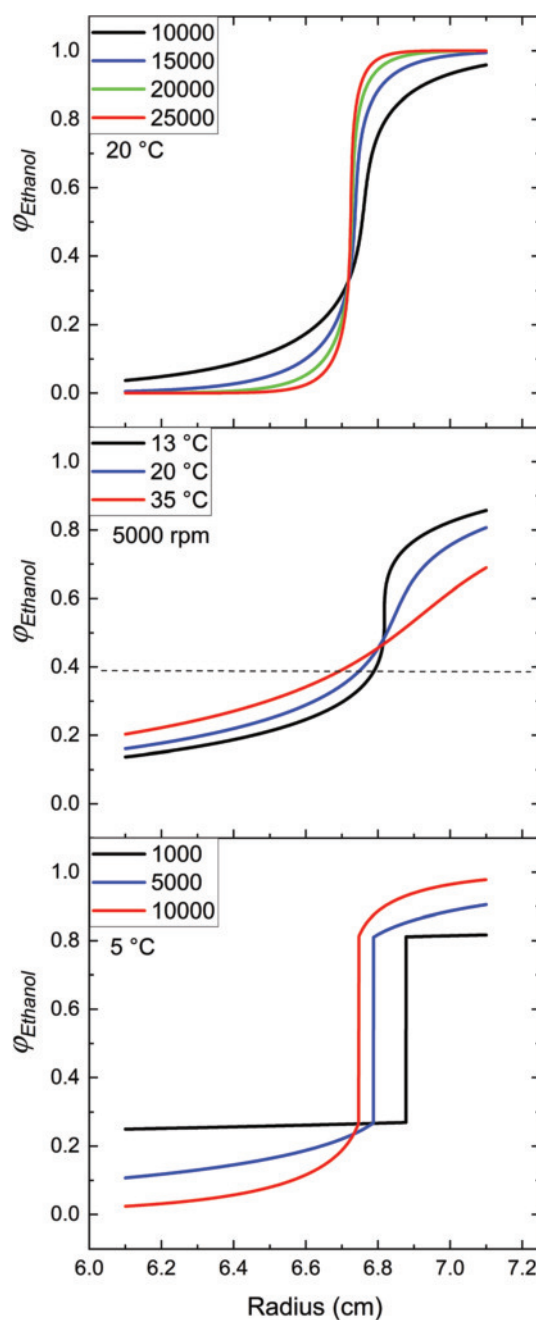


Fig. 8 Concentration changes during centrifugation above (top, middle) and below (bottom) the critical temperature. The dodecane/ethanol weight ratio is 60/40 and the distance from the rotation axis corresponds to the experiment. Top: $T = 20$ °C and the rotation speeds are increased from 10 000 rpm to 15 000, 20 000 and 25 000 rpm. Middle: the rotation speed is 5000 rpm and temperatures are decreased from 35 °C (red) to 20 °C and 13 °C. The dashed line is the average composition of the sample. Bottom: $T = 5$ °C and rotation speeds are decreased from 10 000 rpm (red) to 5000 and 1000 rpm. The critical temperature of the model is 13 °C. The position of the transition between the phases is determined by the Maxwell construction as shown in Fig. S8 (ESI†).

situations. The FH predictions agree qualitatively very well with the experimental observations, but the predicted slopes are higher than in experiment. Above the critical temperature, a single phase is obtained. Increase of the rotation speed (Fig. 8 top) or decrease of temperature (Fig. 8 middle) leads to steeper gradients in composition. Nevertheless, the sample is always within a single phase.

Below the critical temperature (Fig. 8 bottom) there are two separate fluid phases. Centrifugation leads to concentration gradients in each of the fluid phases. A change in the rotational velocity leads a shift of the phase boundary along the radial axis. Remarkably, the compositions of the two fluids at the phase boundary are always the same and equal to the composition of two coexisting phases in the static case at the same temperature. The composition at the phase boundary does not change with speed. The profile changes with speed, and the transition position shifts along the sample but the discontinuity is always the same.

At the critical temperature, under centrifugation we find the critical point transition induced by centrifugation, even though the sample is not at the overall critical composition. As the centrifugation induces a profile of varying composition along the radial axis, the critical composition is locally present at a certain position. At this position, which shifts with changes in the rotational speed, the critical point transition occurs, as shown in Fig. 9. We label this observation centrifuge-induced criticality in samples away from the critical composition. The critical transition is accompanied by critical fluctuations, which are shown in Fig. 10.

Origin of the centrifuge-induced criticality

In the case of a physical system under centrifugation, a single-phase sample will assume a range of densities or a range of

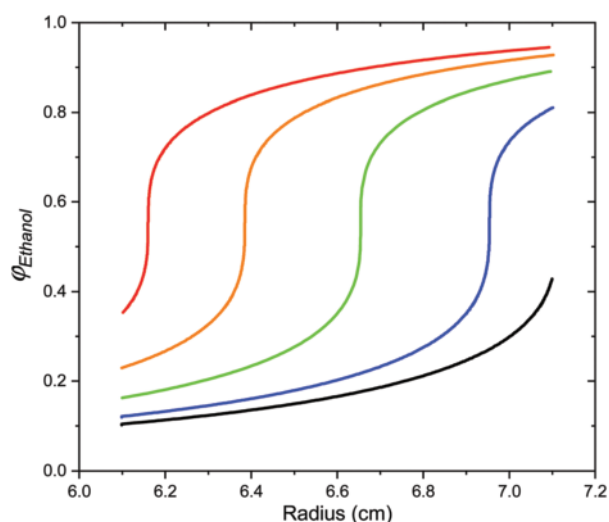


Fig. 9 Demonstration that close the critical temperature we almost always find a region of critical fluctuations. Different compositions are shown in the figure, and the critical region will be absent only when the concentration of one component is very small and the appropriate density is never reached. In this example, $T = 13\text{ }^{\circ}\text{C}$ and the rotation speed is 5000 rpm. The ethanol volume fractions are 0.84, 0.68, 0.50, 0.30, and 0.19 from left to right.

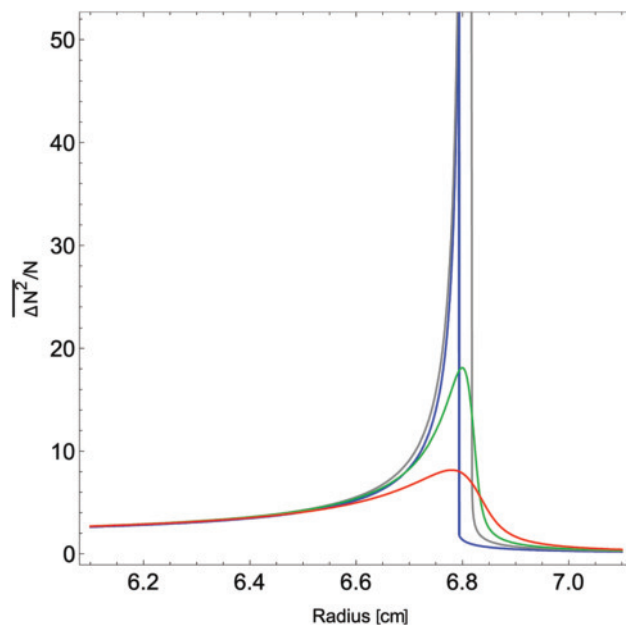


Fig. 10 Fluctuation intensity as a function of position close to the critical temperature at a speed of 5000 rpm. Temperatures are $35\text{ }^{\circ}\text{C}$ (red), $20\text{ }^{\circ}\text{C}$ (green), the critical temperature of $13\text{ }^{\circ}\text{C}$ (grey), and $9\text{ }^{\circ}\text{C}$ (blue). The fluctuations are largest at the critical temperature, in which case the critical transition region can be experimentally recognised by very large composition fluctuation that lead to a broad turbid band as interphase.

compositions. In a theory where the free energy density is a functional only of the local density or composition, at each position in the centrifuged sample, the phenomena like critical fluctuations or phase separation will mimic the behaviour of the stationary system at the same density. This conclusion does not depend on the Flory–Huggins model or the binary fluid phase transition. It will be seen with any similar mean-field model, where centrifugation leads to a range of densities and compositions, for example for a van der Waals fluid describing the liquid vapour phase transition. Beyond a mean field description with the LDA functional we do not expect that this property is exactly valid, but the deviations should be restricted by the range of correlations at the corresponding first-order phase transition.

The spread of values for one controlling variable under the influence of a gravitational field induced by centrifugation can lead to critical phenomena at the critical temperature in a sample, which has a composition other than the critical composition. The phenomenon of centrifuge-induced criticality appears at the critical temperature, but is not restricted to the critical composition or critical density.

The dependence of the physical state of the sample on composition (or density) along the sample in the centrifuge and on the temperature leads to the division of the phase space into three regions, as shown on Fig. 11.

At the blue line (critical temperature) one finds critical behaviour at the point in the sample corresponding to critical composition or density. Thus, even if at the beginning of the experiment the composition is not set to the critical point

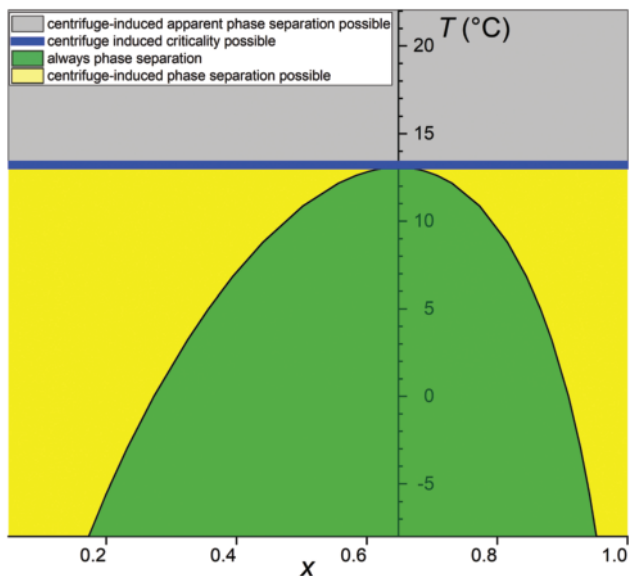


Fig. 11 Temperature-composition plot locating the different behaviours. Within the Flory model, above the critical temperature (top, grey), the slope of the density profile increases with rotational speed and decreases with temperature. The profile between the dense and the dilute end does not cross a singularity but may reach exceedingly high slopes at high rotational speeds. Because of thermodynamical density fluctuations, a turbidity zone a few millimetres thick, similar to critical opalescence, separates the two domains. For all practical purposes, such profiles are seen as a phase separation. The blue line shows the sample at the critical temperature, where critical behaviour can be induced in the centrifuge even if the overall composition does not match the critical composition. In the green region, there are always two coexisting phases. On the left and right of the green two-phase region is a region shown in yellow, in which the sample will split into a two-phase state if the rotation speed is sufficiently high and/or the sample dimension in the radial direction is sufficiently large. In a different context, the dependence of a colloidal interface on the sample dimension was noted earlier.^{36,37}

value, some distance from the rotation axis of the sample the composition will pass through this value and strong fluctuations will lead to critical opalescence. If initial composition is very asymmetrical, this point may lie outside of the experimental range. The critical region is experimentally detectable by the increased turbidity in the sample. If the system is exactly at the critical point in the absence of a centrifugal field, centrifugation will attenuate the criticality in the overall system, since the induced concentration gradients will lead to the appearance of a concentration profile similar to the ones observed for centrifuge-induced criticality.

On the left and right of the green two-phase region (yellow in Fig. 11), at sufficient rotational speeds the sample still splits into a two-phase state. The compositions at the discontinuity are the same as in the static case at the same temperature. In the green region, the sample is always in a two-phase state. However, the position of the meniscus, resp. turbid zone can slightly vary with rotational speed, as can be seen in Fig. 4. As represented in Fig. 10, large important density fluctuations still appear below the critical temperature around the discontinuity.

Comparing experimental results, shown in Fig. 12 to the shift of the turbid zone, shown in Fig. 9, one sees there is a



Fig. 12 Experimentally obtained interference fringe pattern corresponding to the fluctuation expected from theory as shown in Fig. 10. Raw images obtained, showing the narrow turbidity zone appearing at 5000 rpm far away from the critical point (top) and close to the critical point (bottom). The discontinuity in the fringe pattern is clearly visible as vertical line similar to a meniscus. Fig. S9 in the ESI† shows an overlay of fringe patterns and composition profiles.

qualitative agreement between the model results and the observations. However, the profile variations in the experiment appear to be less gradual. The strong gradients above T_s are almost the same as a discontinuous transition. The gradual changes before and after the transition are weak and comparable to the experimental error. The transition is also indicated in the calculation, but gradual changes are seen before and after. It seems that the Flory–Huggins theory, which is restricted to first-neighbour interaction does not contain sufficiently strong coupling to describe ethanol clustering *etc.* The fit parameters for the number of segments are 1:1.5 for ethanol/dodecane, which must reflect strong coupling between ethanol molecules.

Conclusion and outlook

To illustrate the intensity of the effect of the here observed concentration gradients, we evaluated the molar mass of ethanol in dependence of the radius using eqn (9). The routine data interpretation procedure assuming that the gradients obtained 1 °C above the phase boundary are due to the mass of aggregating solute ethanol is shown in Fig. 13.

The order of magnitude of the effect is tremendous. The apparent weight-averaged molar mass of ethanol is in the range of 2500–25 000 g mol⁻¹. This corresponds to an aggregate size of 55–540 molecules of ethanol, which is very large considering the low speed of only 5000 rpm (2000 g), which leads to an ethanol concentration gradient ranging from 36 to 42 wt% (Fig. 13). This shows that near the critical point, even in a low speed centrifuge spinning at a few thousand rpm, a concentration gradient for a small molecule like ethanol can be reached, which would not be possible to reach even applying the best available ultracentrifuges. This shows that soft

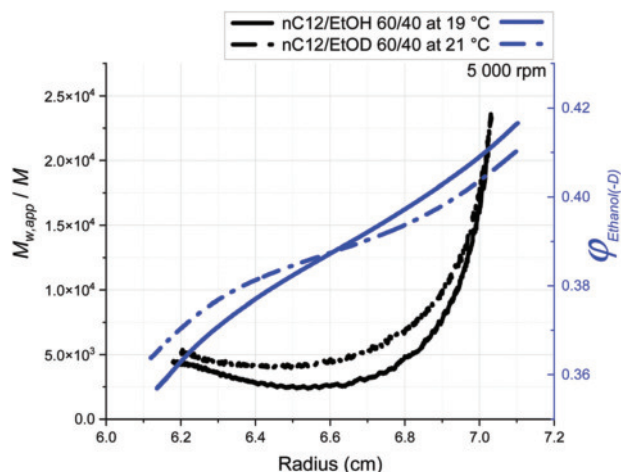


Fig. 13 The apparent weight-averaged molar mass of ethanol, derived via eqn (9) (left hand vertical scale, black), and ethanol volume fraction (right hand vertical scale, blue) versus radius. The value is orders of magnitude higher than the real molar mass of ethanol and moreover it is not constant along the tube. This reflects the interplay between the local centrifugal field and composition.

centrifugation is possible near in temperature but even far in composition from the UCST. Unlike initially believed since the pioneering work of Barden and co-workers, the presence of a well-defined interface is not necessary to observe a broad turbid band instead of the meniscus. Qualitatively, the binary system explored in this paper behaves similarly to an ultra-flexible microemulsion (alias surfactant-free microemulsion), but only near the critical point. The next point to explore is the behavior of ternary systems used in liquid-liquid extraction processes.³⁸ The behavior is qualitatively different in the case of a flexible microemulsion, as described initially in the seventies.^{5,39} To the best of our knowledge, rigid microemulsions have low sensitivity versus temperature and their behavior in centrifugal fields has never been described.

Conflicts of interest

There are no conflicts to declare.

Acknowledgements

This work could only be done via support of the French-German LIA "NISI". SM acknowledges the ERC REE-CYCLE by the European Research Council project "Rare earth recycling with low harmful emissions" No. 320915.

References

- J. Perrin, *Les Atomes*, Félix Alcan, Paris, 1913.
- T. Cao, G. Trefalt and M. Borkovec, *Langmuir*, 2018, **34**, 14368–14377.
- R. H. French, *et al.*, *Rev. Mod. Phys.*, 2010, **82**, 1887–1944.
- V. Reus, L. Belloni, T. Zemb, N. Lutterbach and H. Versmold, *Colloids Surf., A*, 1999, **151**, 449–460.
- R. N. Hwan, C. A. Miller and T. Fort, *J. Colloid Interface Sci.*, 1979, **68**, 221–234.
- S. Bulut, I. Åslund, D. Topgaard, H. Wennerström and U. Olsson, *Soft Matter*, 2010, **6**, 4520–4527.
- K. Ishikawa, M. Behrens, S. Eriksson, D. Topgaard, U. Olsson and H. Wennerström, *J. Phys. Chem. B*, 2016, **30**, 6074–6079.
- M. G. Page, T. Zemb, M. Dubois and H. Coelfen, *Chem-PhysChem*, 2008, **9**, 882–890.
- G. D. Smith, C. E. Donelan and R. E. Barden, *J. Colloid Interface Sci.*, 1977, **60**, 488–496.
- S. C. Greer, T. E. Block and C. M. Knobler, *Phys. Rev. Lett.*, 1975, **34**, 250–253.
- M. R. Moldover, J. V. Sengers, R. W. Gammon and R. J. Hocken, *Rev. Mod. Phys.*, 1979, **51**, 79–99.
- W. R. Rossen, H. T. Davis and L. E. Scriven, *J. Colloid Interface Sci.*, 1986, **113**, 269–287.
- J. Winnick, C. M. Knobler and R. L. Scott, *Phys. A*, 1989, **156**, 77–91.
- J. Pearson, J. Walter, W. Peukert and H. Cölfen, *Anal. Chem.*, 2018, **90**, 1280–1291.
- <https://www.nanolytics-instruments.de>.
- S. Bhattacharyya, P. Maciejewska, L. Börger, M. Stadler, A. Gülsün, H. Cicek and H. Cölfen, *Prog. Colloid Polym. Sci.*, 2006, **131**, 9–22.
- H. Strauss, E. Karabudak, S. Bhattacharyya, A. Kretzschmar, W. Wohlleben and H. Cölfen, *Colloid Polym. Sci.*, 2008, **286**, 121–128.
- OriginLab 2019 software version 9.6.0.172, OriginLab Corporation.
- LabVIEW 2018, 32 bit from National Instruments.
- T. M. Laue On-line data acquisition and analysis from the Rayleigh interferometer, in *Analytical Ultracentrifugation in Biochemistry and Polymer Science*, ed. S. E. Harding, A. J. Rowe and J. C. Horton, The Royal Society of Chemistry, Cambridge, 1992, pp. 63–89.
- W. Mächtle and L. Börger, *Analytical ultracentrifugation of polymers and nanoparticles*, Springer, 2006.
- W. Heller, *J. Phys. Chem.*, 1965, **69**, 1123–1129.
- P. J. Flory, *Principles of Polymer Chemistry*, Cornell University Press, Ithaca, NY, 1953, chap. XII.
- R. Evans, The nature of the liquid-vapour interface and other topics in the statistical mechanics of non-uniform, classical fluids, *Adv. Phys.*, 1979, **28**, 143–200.
- D. Henderson *Fundamentals of Inhomogeneous Fluids*, Dekker, 1992.
- Y. Tsori and L. Leibler, *C. R. Phys.*, 2007, **8**, 955–960.
- J.-P. Hansen and I. R. McDonald *Theory of Simple Liquids*, Academic Press, 1986.
- H. K. Leung and B. N. Miller, *Phys. Rev. A: At., Mol., Opt. Phys.*, 1975, **12**, 2162–2167.
- A. Onuki and H. Kitamura, *J. Chem. Phys.*, 2004, **121**, 3143–3151.
- J. Frenkel, *J. Chem. Phys.*, 1939, **7**, 538–547.

- 31 A. Ben Naim *Solvation Thermodynamics*, Springer, 1987.
- 32 M. Schmidt, M. Dijkstra and J.-P. Hansen, *J. Phys.: Condens. Matter*, 2004, **16**, S4185–S4194.
- 33 M. Tomšič, A. Jamnik, G. Fritz-Popovski, O. Glatter and L. Vlček, *J. Phys. Chem. B*, 2007, **111**, 1738–1751.
- 34 B. Moeser and D. Horinek, *Biophys. Chem.*, 2015, **196**, 68–76.
- 35 O. Sonnevile-Aubrun, V. Bergeron, T. Gulik-Krzywicki, B. Jönsson, H. Wennerström, P. Lindner and B. Cabane, *Langmuir*, 2000, **4**, 1566–1579.
- 36 E. A. G. Jamie, H. H. Wensink and D. G. A. L. Aarts, *Soft Matter*, 2010, **6**, 250–255.
- 37 E. A. G. Jamie, H. H. Wensink and D. G. A. L. Aarts, *J. Stat. Mech.*, 2010, **11008**.
- 38 ZVI Ludmer, Lemaire Aubry HCPE, Pellet-Rostaing, Zemb, Pleines, Kunz, European patent 17 01 2020 number: 20 305 039.8.
- 39 M. Dvolaitzky, M. Guyot, M. Lagües, J. P. Le Pesant, R. Ober, C. Sauterey and C. Taupin, *J. Chem. Phys.*, 1978, **69**, 3279–3288.